Proceedings of the Linear Accelerator Conference 1990, Albuquerque, New Mexico, USA

Induction Acceleration Module for Maryland Pulse Compression Experiment*

J. G. Wang, D. X. Wang, E. Boggasch[a], D. Kehne, M. Reiser, and T. Shea[b]
Laboratory for Plasma Research and Department of Electrical Engineering
University of Maryland, College Park, MD 20742

Abstract

A compact induction acceleration module has been designed and constructed for the electron pulse compression experiment at the University of Maryland. The design parameters, operation principle and performance characteristics of this device are briefly reported in this paper.

Introduction

The Maryland Electron Pulse Compression Experiment[1] requires a fast electron beam pulse with quadratically time-dependent energy shear. This is achieved by an electron beam injector that consists of a variable-perveance gridded electron gun, three solenoidal matching lenses and an induction acceleration module. The electron gun[2] produces a beam with 50 ns pulse width, 40 mA current and 2.5 keV energy. The induction acceleration module produces a voltage that varies as a quadratic function with time from 0 to 5 kV across its gap. This voltage imparts an approximately linear head-to-tail velocity shear to the beam electrons to cause compression. In this report we present the induction acceleration module design, its operating principle, modulator circuit analysis, and some test results.

Induction acceleration module

A toroidal ring of magnetic material surrounded by a conducting loop is driven by a voltage pulse from a modulator, and the change in flux in the magnetic core induces an axial electric field[3,4]. The voltage appearing across a gap in a second loop during the flux change is expressed by

$$V_g(t) = \oint E \cdot dl = -\iint \frac{dB}{dt} \cdot ds \qquad (1)$$

where the accelerating particles perform the line integration and the surface integral is taken over the cross section of the ferromagnetic material. The gap voltage will drop dramatically if the toroidal core material reaches magnetic saturation. Assuming a t^2 gap voltage during operation, Eq. (1) yields

$$V_{g,max}\,\tau = 3\,A\,\Delta B \qquad (2)$$

which relates the maximum gap voltage, the core cross-sectional area A, the total change in the magnetic flux density, ΔB, and the maximum operation time τ before the core saturation.

As illustrated in Fig. 1, the induction acceleration module consists of a single-turn primary around 2 soft ferrite cores (H material) with the beam completing the single-turn secondary. This arrangement forms an inductively isolated gap with a one-to-one voltage ratio. The primary is driven symmetrically from two opposite sides in a balanced mode to minimize deflections of the beam. The beam tube has a radius of 1.9 cm and the gap distance is 4 mm. The dimensions of each ferrite are 14.82 cm in outer diameter, 6.35 cm in inner diameter and 1.59 cm in width. The total cross-sectional area of the core is 13.45 cm^2. The saturation flux density B_s of the material is 0.34 Tesla. Taking the maximum gap voltage of 5 kV at τ=50 ns, Eq. (2) yields the maximum change of the magnetic flux density of $\Delta B \approx 0.06$ Tesla which is much smaller than the saturation flux density of the material. It is expected that the first quadrant of the B-H curve of the material is adequate for operation. Nevertheless, the gap voltage will swing up to a higher value after the 50 ns beam pulse period, that could drive the core into saturation. Since the material has a residual magnetism B_r of 0.15 Tesla, one needs a reversal current after each shot to restore the core approximately to the origin of its B-H curve.

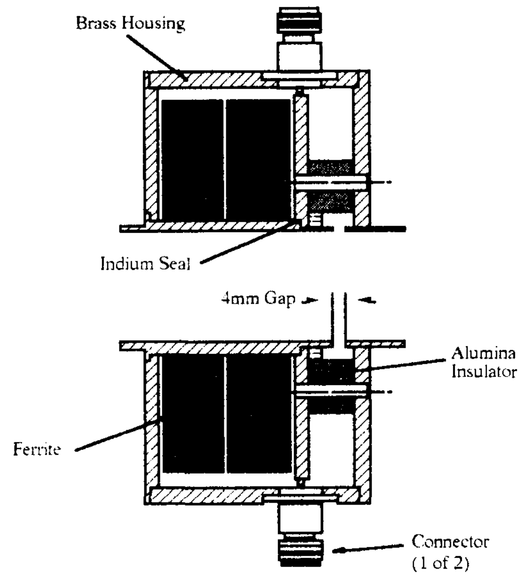

Fig. 1. Mechanical drawing of the induction acceleration module.

Since the gap voltage V_g is quadratically time-dependent, the gap physical characteristics will rely on this feature. For instance, the longitudinal impedance of the acceleration gap will vary in a large range during the beam pulse. The very low impedance at the beam front results in heavy load problem and waveform distortion. The acceleration gap acting on the beam as a focusing lens will also produce severe chromatic aberrations that cause problems with beam matching to the periodic focusing channel and may also lead to emittance growth.

Modulator

The schematic diagram of the induction acceleration module and its associated modulator circuits is shown in Fig. 2. The induction acceleration module itself is equivalent to a RLC parallel circuit where R accounts for the resistive loss in the core. With the external capacitance and inductance, the five components C_1, L_1, C_2, L_2, and R constitute a Pulse Forming Network (PFN).

The behavior of the PFN is governed by a fourth-order differential equation. In the complex frequency domain the

* Research Supported by the U.S. Department of Energy
[a] GSI Darmstadt, W. Germany
[b] Brookhaven National Laboratory

voltage on the induction module is related to the charging voltage V_0 on the capacitor C_1 by

$$V(s) = \frac{V_0 \omega_3^2 s}{s^4 + s^3 \omega_0 + s^2\left(\omega_1^2 + \omega_2^2 + \omega_3^2\right) + s\omega_0\omega_1^2 + \omega_1^2\omega_2^2}, \tag{3}$$

where the characteristic frequency constants ω_0 thru ω_3 are determined by the PNF parameters RC_2, L_1C_1, L_2C_2, and L_1C_2, respectively. Transforming Eq. (3) back to the time domain is straightforward, and one finds the induction gap voltage as

$$V(t) = V_0\omega_3^2 p e^{-at}\left[\cos(bt) + \frac{q - ap}{bp}\sin(bt)\right] - V_0\omega_3^2 p e^{-ct}\left[\cos(dt) + \frac{r - cp}{dp}\sin(dt)\right], \tag{4}$$

where the constants a, b, c, d, and p, q, r are determined by the PNF parameters. For a small time scale t, equation (4) can be approximated as

$$V(t) \approx \frac{1}{2} V_0 \left(\omega_3 t\right)^2 . \tag{5}$$

This proves that under certain conditions the induction acceleration module with the driving modulator circuit does lead to a quadratically time-dependent voltage.

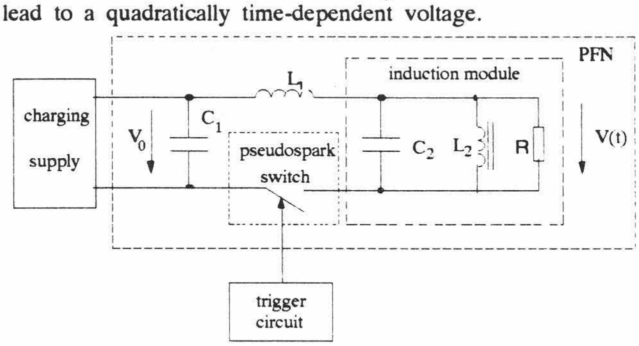

Fig. 2. Schematic diagram of the induction acceleration module and its modulator.

Ignoring the resistive loss of the core, the current through the induction acceleration module can be found as

$$i(t) = \frac{V_0 C_2 \omega_3^2}{\left(d^2 - b^2\right)}\left[\frac{\left(d^2 - \omega_2^2\right)}{d}\sin(dt) + \frac{\left(\omega_2^2 - b^2\right)}{b}\sin(bt)\right] \tag{6}$$

Equation (6) shows that the current through the induction acceleration module is sinusoidal. With the proper switch that allows current reversal, the cores will be degaussed after each shot and the induction acceleration could be operated without a separate reset circuit.

Pseudospark switch

A pseudospark switch is employed to control the PFN operation. The pseudospark discharge switch[5] is a fast, spark-like, low-pressure gas discharge that operates on the left side of the Paschen curve. A gap geometry that supports the pseudospark discharge consists of two insulated metal electrodes with a center hole. The discharge can be triggered at the cathode by a flashover initiated inside the bore hole across a thin mylar surface. Table 1 shows the typical operating parameters for this switch. This data set indicates superior performance of the switch in the aspects of fast risetime, small jitter, repetition rate and long lifetime. The tests show that the pseudospark switch has current reversal ability when the charging voltage V_0 is more than 6 kV.

Table 1
Operating Parameters of the Pseudospark Switch

Hold-off voltage	20 kV
Current	10 kA
Current rise (max.)	500 A/ns
Jitter	1 ns
Delay	30 ns
Repetition rate	100 Hz
Gas pressure	30 millitorr
Lifetime	> 1 million shots
Gas type	nitrogen

Test results

The induction acceleration module has been tested with respect to its gap voltage, module current, and circuit behavior. The modulator components used in this test are C_1=2400 pF, L_1=2.3 μH, C_2=2000 pF, and L_2=3.4 μH.

A typical gap voltage waveform taken at the charging voltage of V_0=18 kV is shown in Fig. 3. In the first 50 nanosecond or so, the gap voltage increases quadratically with time during which the electron beam will be synchronized and accelerated. This time dependence gradually disappears at larger time scales when the conditions for Eq. (5) are no longer satisfied. However, this has no effect on beam acceleration. Figure 4 fits the gap voltage data to the ideal t^2 curve, that shows reasonably good agreement between the theory and experimental data. The waveform of the t^2 dependence could be further improved by increasing C_1 or L_1, but that would require a higher charging voltage or lower repetition rate of operation. The measured gap voltage versus the charging voltage V_0 is plotted in Fig. 5 which shows reasonably good linearity of operation.

The current waveform passing through the induction module is shown in Fig. 6. The peak current is about 450 A when the charging voltage is 18 kV. The reverse current has a peak value of approximately 200 A and lasts about 300 ns. This results in a reasonable degauss effect on the core operation. In Fig. 7 the forward and reverse peak current of the induction module as a function of the charging voltage is also plotted. The linear behavior of the forward current indicates that the core is operated without getting into saturation. The nonlinearity of the reverse current explains the current reversibility of the pseudospark only at a higher charging voltage.

Summary

A compact induction acceleration module has been designed and constructed for the Longitudinal Compression Experiment at the University of Maryland. It generates an acceleration gap voltage that varies approximately as a quadratic function of time. This imparts a head-to-tail velocity spread to the electron beam pulse which is injected into a solenoidal focusing channel. The velocity spread will produce longitudinal compression of the electron pulse as it propagates down the 5 m long channel. The induction acceleration module employs a pseudospark switch to achieve good performance in synchronization and current reversibility. The induction acceleration module has been tested and the test results show satisfactory performance of this device. The interaction between the beam and the induction gap will be studied in detail with the new injector and the results will be reported in the near future.

References

1. T. Shea, E. Boggasch, Y. Chen, M. Reiser, "The University of Maryland Electron Pulse Compression Experiment", Proceedings of the IEEE Particle Accel. Conf., Chicago, p.1049, March 1989.
2. J. G. Wang, E. Boggasch, P. Haldman, D. Kehne, M. Reiser, T. Shea, and D. X. Wang, "Performance characteristics of a variable-perveance gridded electron gun", to be published in IEEE Trans. ED.
3. N. C. Christofilos, R. E. Hester, W. A. S. Lamb, D. D. Reagan, W. A. Sherwood, and R. E. Wright, "High current linear induction accelerator for electrons", Rev. Sci. Instrum., **35**(7), 886-890 (1964).
4. James E. Leiss, Neil J. Norris and Mark A. Wilson, "The design and performance of a long-pulse high-current linear induction accelerator at the National Bureau of Standards", Particle Accelerators, **10**, 223-234 (1980).
5. J. Christiansen and C. Schultheiss, Z. Phys. **A290**, 35 (1979).

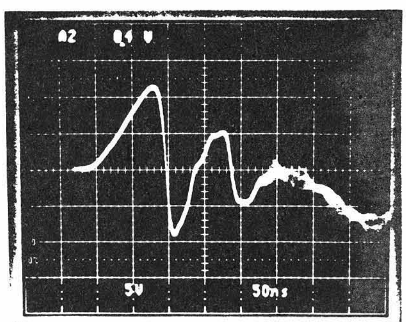

Fig. 3. Measured induction gap voltage waveform at V_0=18 kV which shows a quadratically rising gap voltage at the first 50 ns period (5 kV/div. vertically).

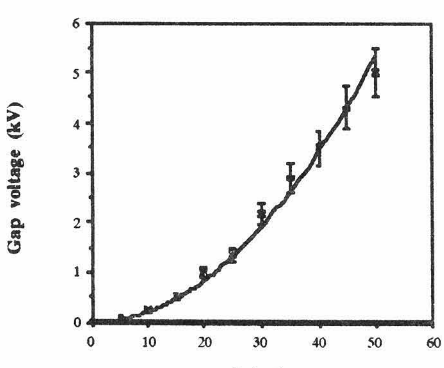

Fig. 4 Gap voltage in the first 50 ns where the smooth curve is a t-square form fitted to the experimental data by least square method.

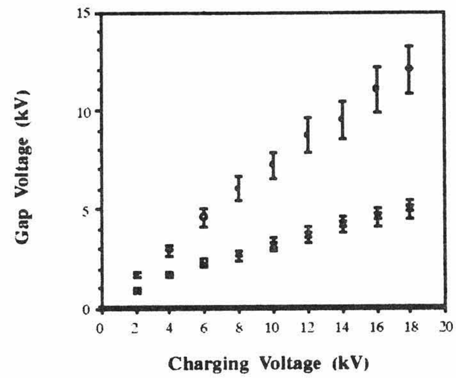

Fig. 5. Gap voltage versus charging voltage V_0 where the top points are the peak gap voltage and the bottom points are the gap voltage at τ=50 ns.

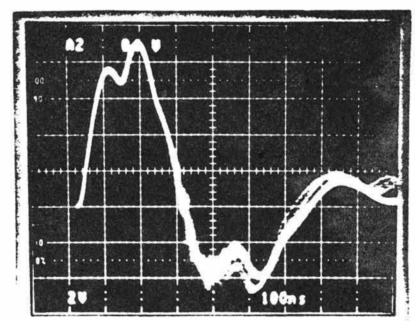

Fig. 6. Induction module current waveform (100 A/div. vertically) at V_0=18 kV which shows the reverse current through the pseudospark switch to reset the core.

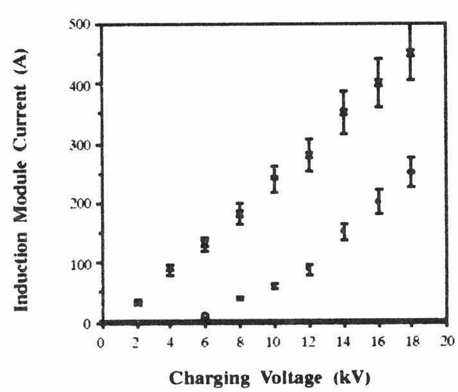

Fig. 7. Induction module current versus charging voltage V_0 where the top points are the peak forward current and the bottom points are the peak reverse current.